Research Paper

Halogenated Salts as Coagulant to Prepare Bovine Serum Albumin Nanoparticles Containing Paclitaxel using High-Pressure Homogenisation Method

YAN CHU, SHUO CHAI, H. PAN, JIAYI QIAN, CUIYAN HAN, X. SUI* AND TINGTING LIU

College of Pharmacy, Qiqihar Medical University, Qiqihar, Heilongjiang 161006, China

Chu *et al.*: Preparation of Bovine Serum Albumin Nanoparticles Containing Paclitaxel using High-Pressure Homogenisation

In this study, bovine serum albumin-paclitaxel nanoparticles were prepared by high-pressure homogenization method with halogenated salt as coagulant. The effect of process parameters such as bovine serum albumin concentration, coagulant concentration, homogenisation time, homogenisation pressure, water/ethanol ratio and bovine serum albumin-paclitaxel ratio was analyzed to optimize nanoparticle size, bovine serum albumin conversion rate and encapsulation efficiency. Bovine serum albumin concentration and homogenisation pressure were found to exert a great influence on bovine serum albumin conversion rate and particle size. Meanwhile, the bovine serum albumin-paclitaxel ratio significantly affected the nanoparticle encapsulation efficiency. Electron microscopy showed that the freeze-dried particles mostly existed in the form of dimers and trimers with an average particle size of 300-400 nm. Infrared spectroscopy indicated that paclitaxel was well encapsulated in bovine serum albumin. Raman spectra of the synthesized nanoparticles indicated changes in the disulphide bond configuration and protein structure. In addition, the effect of different crosslinking agents (genipin, vanillin and glutaraldehyde) on drug release from the nanoparticles in *in vitro* conditions was investigated. The study confirmed vanillin had better sustained release effect. These results suggest that high-pressure homogenization method with halogenated salts as coagulant is an effective method to prepare drug-delivery systems with albumin as a carrier.

Key words: Albumin nanoparticles, paclitaxel, high pressure homogenization, halogenated salts, green chemistry

Nanoparticle-based drug-delivery systems are considered to show great potential for cancer treatment as these carrier systems exhibit high drug absorption, adjustable drug-release rate and targeted delivery, especially in the case of hydrophobic drugs[1]. Previous reports have suggested that nanoparticles hundreds of nanometers in diameter can passively reach tumors by virtue of the Enhanced Permeability and Retention (EPR) effect[2,3]. Lately, nanoparticle drug-delivery systems with albumin as a carrier are receiving much attention. As an endogenous substance, albumin plays a unique role in reducing the phagocytosis of nanoparticles, thus prolonging the *in vivo* circulation of drugs[4,5]. In addition, albumin is a macromolecular carrier, whose pores can encapsulate hydrophobic compounds. Moreover, albumin can be tightly but reversibly bound to certain drugs through non-covalent bonds to realize drug transport *in vivo* and their release at the target cell surface[6]. Bovine Serum Albumin (BSA) is one of the most commonly used drug carrier proteins owing to its good biocompatibility, low cost and easy purification[7]. BSA based nanoparticle drug-delivery systems exhibit various functions and binding properties such as good stability and a high binding capacity for drugs with different physical and chemical properties.

Traditionally, albumin nanoparticles are mainly prepared by emulsification and desolation[8]. The emulsification technique for the production of albumin nanoparticles involves the emulsification of albumin solution in an oil phase and solidification by chemical cross-linking. In Bomi Kim study fabricated an albumin nanoparticle formulation for co-loading Paclitaxel (PTX) and curcumin using chloroform as the solvent[9]. The process need to use toxic organic solvents such as dichloromethane and

***Address for correspondence**
E-mail: suixiaoyu@outlook.com

Accepted 08 August 2022
Revised 25 October 2021
Received 19 July 2021
Indian J Pharm Sci 2022;84(4):1013-1025

chloroform, which may lead to adverse health effects. The preparation of nanoparticles with long period and the difficulty of controlling the albumin particles size. Using the desolation method, nanoparticles are obtained by continuously dropping a water-miscible organic phase such as ethanol into an aqueous albumin solution under continuous stirring until the solution becomes turbid[10]. The formed nanoparticles are wide size distribution. In this process, albumin generally does not undergo denaturation (water-soluble substance) and does not have sustained release effect, which requires hardening by crosslinking with chemical cross linkers, such as glutaraldehyde or methanol. During this process, however, bioactive macromolecules may be deactivated and residues of harmful solvents may be formed[11].

Green chemistry is a powerful ally of the pharmaceutical industry[12]. To synthesize nanoparticles in a 'green' manner, a non-toxic solvent medium should be used; in addition, non-toxic materials should be used to stabilize these nanoparticles[13]. Most of the preparation methods reported thus far rely heavily on organic solvents, which leads to toxicity[14,15]. In this study, we prepared BSA-PTX nanoparticles using halogenated salts as coagulants by high-pressure homogenization technique. On one hand, nanoparticles prepared by high-pressure homogenization technology have the advantages of small particle size and uniform size distribution; simultaneously, superoxide dismutase, produced by high-pressure homogeneous cavitation, was used to promote the formation of disulphide bonds between the cysteine residues of protein molecules. On the other hand, because in the process of preparation, coagulation and dispersion can be achieved at the same time, it is a high-efficiency preparation technology. The size and entrapment efficiency of the nanoparticles were analyzed along with their physical and chemical properties. The *in vitro* release characteristics of nanoparticles obtained by secondary curing with different crosslinking agents were compared.

MATERIALS AND METHODS

PTX, calcium lactate and gluconolactone were procured from Dalian Meilun Biology Technology Co., Ltd. (Dalian, China). BSA, calcium chloride and Magnesium chloride ($MgCl_2$) were purchased from Sigma Aldrich Co. Ltd. (Shanghai, China) and methanol was purchased from J&K Scientific Ltd. (Beijing, China). Ethanol and dichloromethane were purchased from Sino pharm Chemical Reagent Co. Ltd. (Beijing, China). Pure water was prepared using a Milli-Q water purification system (Millipore, Bedford, MA, United States of America (USA)).

Preparation of albumin nanoparticles:

The schematic diagram of the experimental apparatus was shown in fig. 1. An albumin solution was prepared by dissolving 20 mg of the coagulant ($MgCl_2$) and 400 mg of BSA in 40 ml (50°) of pure water. Meanwhile, 40 mg of PTX was dissolved in ethanol. The albumin solution was slowly added to the material cup of a high-pressure homogenizer and the temperature of the circulating water bath was set at 50°. PTX solution was added drop wise (1 ml/min) to this pre-heated albumin solution at a pressure of 150 bars. Subsequently, the homogenisation pressure was adjusted to the target value and after a set time period, drug-loaded albumin nanoparticle suspensions could be obtained. These solutions were centrifuged at 8000 rpm for 8 min in an ultracentrifuge (CP70MX, Hitachi Koki Co. Ltd., Japan) and the supernatant was removed. The precipitates were washed twice with 75 % ethanol to remove free PTX. Later, the obtained precipitates were lyophilised with cryoprotectant mannitol (1:1 mass ratio). After pre-freezing for 12 h at -80°, the nanoparticles were freeze-dried at a shelf temperature of -50° for 24 h at a chamber pressure of 1-20 Pa in a lyophilizer (SJIA-10N, Ningbo Shuangjia Science Technology Development Co. Ltd., China).

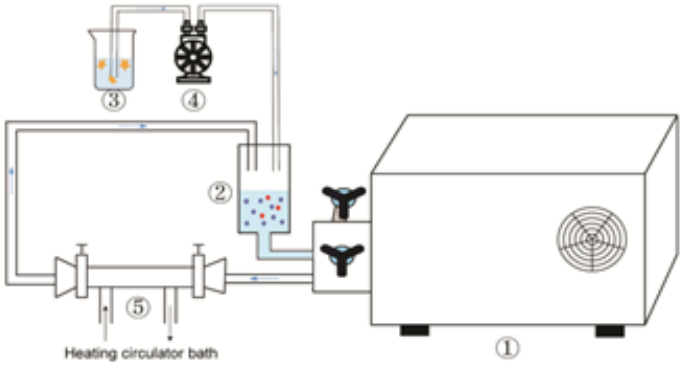

Fig. 1: Schematic diagram of the experimental apparatus, (1): High pressure homogenizer; (2): Material cup; (3): Drug solution; (4): Peristaltic pump and (5): Heating circulator bath

Preparation of cross linked albumin nanoparticles:

An albumin-nanoparticle suspension was prepared as described in above, centrifuged at 8000 rpm for 8 min using an ultracentrifuge (CP70MX, Hitachi Koki Co. Ltd., Japan) and the supernatant was removed. Purified water (6 ml) was added to the reaction flask to disperse the precipitate. Three crosslinking agents (genipin, vanillin and glutaraldehyde) were added to this dispersion and allowed to react for 90 min at 60°. Subsequently, the precipitates were lyophilised with cryoprotectant mannitol (1:1 mass ratio). After prefreezing for 12 h at -80°, freeze-drying was carried out at a shelf temperature of -50° for 24 h at a chamber pressure of 1-20 Pa in a lyophiliser (SJIA-10 N, Ningbo Shuangjia Science Technology Development Co. Ltd., China).

Quantitative determination of PTX using High-Performance Liquid Chromatography (HPLC):

PTX content was analyzed on a C_{18} HPLC column (250×4.6 mm^2, 5 µm; Shandong Lunan Ruihong Chemical Instrument Co. Ltd.) with methanol and water (75:25 v/v) as mobile phase A and methanol (100 %) as mobile phase B (100 %) at a flow rate of 1.0 ml/min. The analyses were evaluated using a wavelength detector at 227 nm. The injection volume was set at 20 µl. A linear regression equation, y=0.6913x+5.925 (R^2=0.9995), where "y" indicates peak area and "x" represents mass concentration, was observed in the range of 10-100 µg/ml, illustrating a good linear relationship.

Determination of PTX encapsulation efficiency:

The prepared BSA-PTX solution (320 µl) was pipetted into a centrifuge tube and to this solution, 2 ml of dichloromethane was added and vortexed for 5 min; the solution was then left to equilibrate for 15 min. The obtained solution was filtered through a 0.22 µm syringe filter and transferred to a 1 ml penicillin bottle. The ultra-filtrate (20 µl) was injected into the HPLC system and analyzed at an Ultraviolet (UV) absorption wavelength of 227 nm; the content of PTX detected was called the content of free drug. Encapsulation efficiency was calculated according to the following equation

$$\text{Encapsulation efficiency (\%)} = W_{total} - W_{free} / W_{total} \quad (1)$$

Where W_{free} is the amount of free drug and W_{total} is the amount of total drug.

Determination of the conversion rate of albumin:

The BSA-PTX nanoparticle suspension (4 ml) was pipetted into a centrifuge tube and centrifuged at 10 000 rpm for 30 min at 4°. Subsequently, 50 µl of the supernatant was pipetted out and added to 1950 µl of purified water. The UV absorption of this solution was measured at 227 nm and the corresponding chromatogram was recorded. The recorded value represents absorbance by free albumin and was used to calculate the conversion of BSA-PTX nanoparticles. A linear regression equation, y=0.632x+0.0245 (R^2=0.9991) was obtained, where the absorbance (y) and albumin concentration (x) exhibited a good linear relationship in the concentration range of 10-100 µg/ml. The Albumin Conversion Rate (ACR) was calculated according to the following equation:

$$\text{ACR (\%)} = W_{total} - W_{free} / W_{total} \quad (2)$$

Where W_{free} is the amount of free albumin and W_{total} is the amount of total albumin.

Measurement of particle size of nanoparticles:

Albumin nanoparticles powders were dispersed with pure water and their mean size were characterized using a laser particle-size analyzer (Nano ZS90 Malvern Instruments, UK).

Fourier Transform Infrared (FTIR) spectroscopy:

The FTIR spectra of the samples were obtained on a Nicolet 6700 FTIR spectrometer (Thermo Scientific, Waltham, MA, USA). Each sample was mixed with potassium bromide in an agate mortar and compressed into a thin disc to form pelletized specimens. These specimens were scanned in the range of 4000-400 cm^{-1} at a resolution of 4 cm^{-1}.

Raman Spectrometry (RS):

FT-Raman spectra were acquired on a Nicolet 6700 FTIR with NXR FT-Raman module (1064 nm) in the wavenumber range of 4000-400 cm^{-1} over 64 scans with a 4 cm^{-1} spectral resolution.

Differential Scanning Calorimetry (DSC):

DSC measurements were conducted on a High Strength Concrete-1 (HSC-1) DSC scanning calorimeter (Hengjiu Instrument Ltd., Beijing, China). Samples (15 mg) were placed in aluminum pans, sealed using the sample pan press and heated from 25° to 400° at a rate of 10°/min in a nitrogen atmosphere.

X-Ray Diffraction (XRD):

The structural properties of the samples were analyzed using a D8 Focus X-Ray diffractometer (Bruker, Germany) with Cu-Kα radiation operating at 40 kV and

40 mA. The samples were scanned in the 20 range of 3° to 90° at 0.02°/min.

Scanning Electron Microscopy (SEM):

The samples were fixed on a SEM stub with a conductive carbon tape and sputter-coated with a thin layer of gold using an SBC-12 sputter-coater (KYKY Tech. Ltd., Beijing, China). The surface morphology of the samples was then observed using an S-4300 SCM (Hitachi, Tokyo, Japan).

Transmission Electron Microscopy (TEM):

Nanoparticle shape and morphology were observed using a TEM (Hitachi HT7700, Japan) operating at an accelerating voltage of 100 kV. The nanoparticle suspension was obtained by adding 5 mg of nanoparticles powder to 5 ml of purified water at room temperature, vortexed for 10 s and equilibrated for 30 s. From this solution, a drop was withdrawn with a micropipette and placed on a carbon-coated copper grid. Excess suspension was blotted from the grid with a filter paper. The remaining deposit was negatively stained with 1 % phosphotungstic acid (w/w, pH 7.1). The excess was removed with a filter paper and the deposit was dried before analysis.

***In vitro* drug release:**

PTX release from the nanoparticles was analyzed using the slurry method at (37°±0.5°). BSA-PTX nanoparticles were dissolved in 100 ml of a Phosphate Buffer Solution (PBS), (pH 7.4, 37°) by stirring at 100 rpm. At predetermined time intervals, 2 ml of the release medium was removed and replaced with an equal amount of fresh release medium to maintain sink conditions, 2 ml alcohol was added and filtered through a 0.45 μm cellulose acetate membrane. The released drug content was analyzed at 227 nm by HPLC (LC-1000D HPLC, Shandong Lunan Ruihong Chemical Instrument Co. Ltd.). Measurements were carried out in triplicate to calculate cumulative drug release.

Data analysis:

Single correlation analysis was conducted to examine the effect of process parameters on the properties of albumin nanoparticles. All statistical evaluations were conducted with Statistical Package for Social Sciences (SPSS) for Windows, version 17.0.0 (SPSS Inc., USA). A value of $p<0.05$ was considered to be statistically significant.

RESULTS AND DISCUSSION

According to the available literature, intermolecular functional regions can be generated by interactions between protein molecules and divalent metal ions to form precipitates and these precipitates enhance the stability and duration of protein interaction, resulting in a sustained release effect[16]. Moreover, the impact may be caused by the type of coagulant on the crosslinking mechanism and rate, thereby affecting the particle size and conversion rate of albumin nanoparticles. Taking these factors into account, in this study, the effect of different coagulants on the particle size and conversion rate was investigated.

As shown in fig. 2, under the same preparation conditions, the conversion rate of the 50 mg coagulant group (1.25 mg/ml) was higher than that of 20 mg coagulant group (0.5 mg/ml). In terms of the conversion rate in the 0.5 mg/ml coagulant group, the following order was observed-$MgCl_2$>gluconolactone>calcium chloride>calcium lactate, with $MgCl_2$ resulting in the highest conversion rate (47 %). In the case of the 1.25 mg/ml coagulant group, the observed order was $MgCl_2$>gluconolactone>calcium chloride>calcium lactate, with $MgCl_2$ resulting in the highest conversion rate (84.5 %). Significant nanoparticle flocculation was observed when gluconolactone was used as the coagulant, owing to which the nanoparticles could not be effectively dispersed.

The particle size of albumin nanoparticles in the 0.5 mg/ml coagulant group was smaller than that in the 1.25 mg/ml group. Particle-size order in the 0.5 mg/ml coagulant group was $MgCl_2$<calcium chloride<calcium lactate<gluconolactone, with nanoparticles prepared using $MgCl_2$ being the smallest (310.6 nm). In the 1.25 mg/ml coagulant group, the particle-size order was $MgCl_2$<calcium chloride<calcium lactate<gluconolactone, with nanoparticles prepared using $MgCl_2$ being the smallest (398.6 nm).

Thus, considering the particle-size and conversion-rate indicators, $MgCl_2$ was selected as the optimal coagulant and used in the rest of the study.

During the synthesis of albumin nanoparticles by High-Pressure Homogenisation Coagulation Method (HPHCM), nanoparticle size, albumin-conversion rate and encapsulation rate can be adjusted by controlling the operating conditions such as BSA concentration, coagulant dosage and homogenisation time. Therefore, we investigated the effect of different experimental conditions (Table 1) on the quality of the produced nanoparticles.

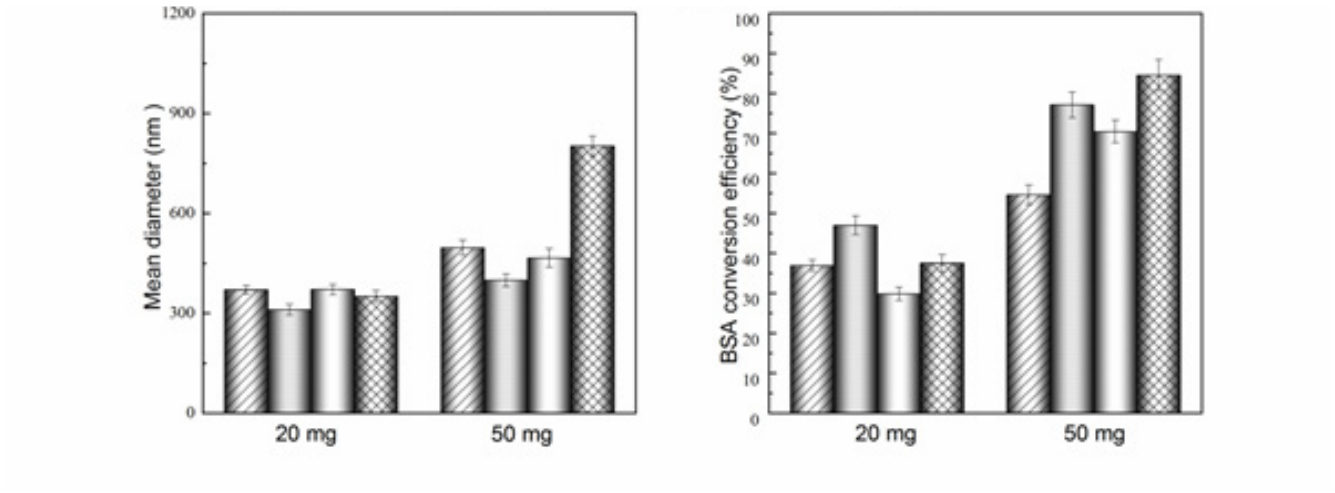

Fig. 2: Influence of coagulant concentration and types of coagulants on the mean particle size and BSA conversion efficiency
Note: ( ): Calcium chloride; ( ): $MgCl_2$; ( ): Calcium lactate and ( ): Gluconolactone

TABLE 1: EXPERIMENTAL CONDITIONS FOR SINGLE FACTOR STUDIES

Influence factors	Level	Other conditions
BSA concentration (mg/ml)	5 10 20 30 40	$MgCl_2$ concentration 0.5 mg/ml, the volume ratio of water and ethanol 30, homogeneous pressure 600 bar, homogeneous time 3 min, mass ratio of BSA and PTX 25
$MgCl_2$ concentration (mg/ml)	0.5 0.75 1 1.25 1.5	BSA concentration 10 mg/ml, the volume ratio of water and ethanol 30, homogeneous pressure 600 bar, homogeneous time 3 min, mass ratio of BSA and PTX 25
The volume ratio of water and ethanol	30 25 20 15 10	BSA concentration 10 mg/ml, $MgCl_2$ concentration 0.5 mg/ml, homogeneous pressure 600 bar, homogeneous time 3 min, mass ratio of BSA and PTX 25
Homogeneous pressure (bar)	600 700 800 900 1000	BSA concentration 10 mg/ml, $MgCl_2$ concentration 0.5 mg/ml, the volume ratio of water and ethanol 20, homogeneous time 3 min, mass ratio of BSA and PTX 25
Homogeneous time (min)	3 6 9 12 15	BSA concentration 10 mg/ml, $MgCl_2$ concentration 0.5 mg/ml, the volume ratio of water and ethanol 20, homogeneous pressure 800 bar, mass ratio of BSA and PTX 25
Mass ratio of BSA and PTX	25 20 15 10 5	BSA concentration 10 mg/ml, $MgCl_2$ concentration 0.5 mg/ml, the volume ratio of water and ethanol 20, homogeneous pressure 800 bar, homogeneous time 3 min

The effect of BSA concentration on the synthesised albumin nanoparticles is illustrated in fig. 3a. As the BSA concentration increased from 5 to 40 mg/ml, particle size gradually increased from 327 to 377 nm. The change in particle size can be explained using the following relationships:

$$J=Aexp^{(-B/(lnS)2)} \quad (3)$$

$$A=N_0\upsilon \quad (4)$$

$$B=(16\pi\sigma^3 Vs^2)/(3k^3t^3) \quad (5)$$

$$v=kt/(3\pi a^3\eta) \quad (6)$$

Where 'S' is the degree of super saturation, 'J' is the nucleation rate, 'N_0' is the initial number of molecules of solute per unit volume, 'υ' is the frequency of molecular transport to the solid-liquid interface, Furthermore, 'k' is the Boltzmann constant and 't' represents temperature. 'σ' indicates interfacial tension at the solid-liquid interface and 'Vs' is the volume of solute molecules. 'η' is the viscosity of the surrounding solution and 'a' is the mean effective diameter of the diffusing species.

Using equation (3), it was found that viscosity increased as the BSA concentration increased. Larger particles were produced by slowing the nucleation due to a reduced protein transport between water and ethanol. In addition, higher protein concentrations led to greater super saturation (equation (4)), resulting in small nuclei. However, there is a greater chance of particle collision due to high super saturation resulting in solidification, thus producing larger nanoparticles[17]. It has been reported by Prajapati *et al.* that coagulation occurs as BSA concentration increases, resulting in larger particles[18]. Albumin conversion initially increased and then decreased, with the highest conversion rate (45.8 %) observed at a BSA concentration of 10 mg/ml. Shu *et al.* described that the conversion rate increased with an increase in BSA concentration in the range of 0.5-3 mg/ml[19]. In the current study, however, the low conversion rate observed at high concentrations may be attributed to the super saturation effect, as described earlier. Meanwhile, the encapsulation efficiency varied from 85.3 % to 90.8 %, with no obvious trend. Statistically, the influence of BSA concentration on particles size was highly significant ($p<0.01$) and exerted a large influence on albumin-conversion rate ($p<0.05$) into nanoparticles.

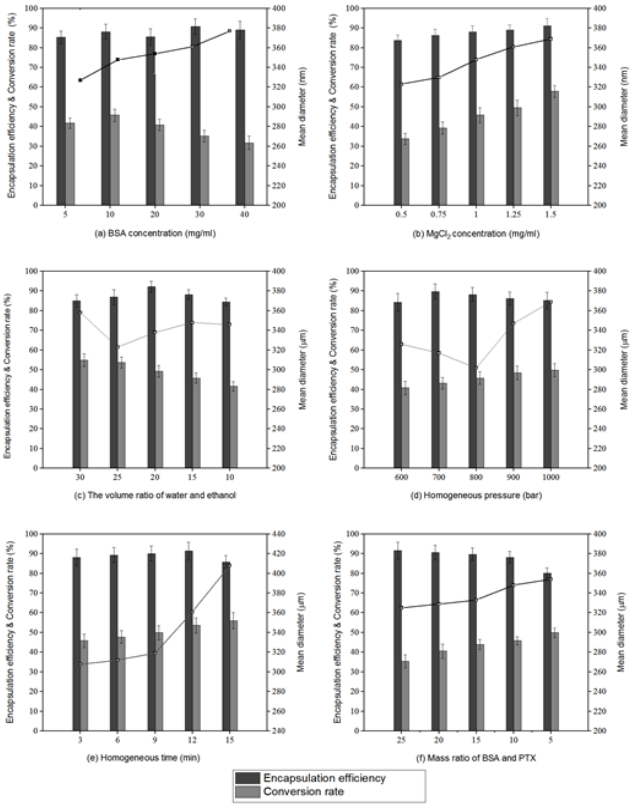

Fig. 3: Influence of (a): BSA concentration (mg/ml); (b): $MgCl_2$ concentration (mg/ml); (c): The volume ratio of water and ethanol; (d): Homogeneous pressure (bar); (e): Homogeneous time (min) and (f): Mass ratio of BSA and PTX on the mean particle size, encapsulation efficiency and total conversion
Note: ( ): Encapsulation efficiency and ( ): Conversion rate

The effect of $MgCl_2$ concentration on the properties of albumin nanoparticles is illustrated in fig. 3b. As the concentration of $MgCl_2$ increased, nanoparticle size, conversion rate, and encapsulation rate increased gradually. An increase in the number of coagulant molecules resulted in an increase in the nucleation rate, which in turn increased the particle size and conversion rate.

The effect of water/ethanol volume ratio on albumin nanoparticles is shown in fig. 3c. As the water/ethanol volume ratio decreased from 30 to 10, the particle size initially decreased and then increased. The minimum particle size of 323 nm was observed at water/ethanol=25/1, which is consistent with previously reported results[20]. Meanwhile, the BSA conversion rate decreased when the water/ethanol volume ratio decreased from 30 to 10. The encapsulation rate initially increased and then decreased and the highest value (92.2 %) was observed at water/ethanol=20/1.

The effect of homogenisation pressure on the properties of BSA nanoparticles is shown in fig. 3d. As the pressure increased from 600 to 1000 bar, particle size initially decreased and then increased, with the smallest particles (302 nm) being obtained at 800 bar. It is well known that a homogeniser gradually warms up during operation and rapid reactant consumption occurs as the reaction rate increases at higher temperatures. As a result, the reactants are depleted, resulting in the formation of smaller nanoparticles at higher temperatures[21]. These results are consistent with those of Jenning *et al.*[22]. Later, the particle size increased gradually due to the exaggerated pressure of the homogeniser, an exorbitant instantaneous energy and the solidification of particles[23]. In this process, the conversion rate also increased. Statistically, the influence of homogenisation pressure on conversion rate was highly significant ($p<0.01$). The encapsulation rate initially increased and then decreased, reaching the highest value (89.7 %) at a homogenisation pressure of 700 bars.

The effect of homogenisation time on albumin nanoparticles is illustrated in fig. 3e. When the homogenisation time increased from 3 to 9 min, the particle size increased gradually while in the range of 9-15 min, it increased rapidly. This phenomenon can be attributed to an energy barrier between the particles. When individual particles approach each other, the potential Attractive Energy (EA) increases rapidly, whereas the potential Repulsive Energy (ER) changes more slowly. Generally speaking, there is a maximum Energy (E_{max}) in the total potential energy curve, which represents the energy barrier and prevents particles from absorbing each other. The E_{max} may overcome when the particles approach each other. As the homogenisation time increases, more and more energy is accumulated. After 9 min, the repulsive potential energy, E_{max} could overcome, owing to which individual nanoparticles were strongly attracted to each other, resulting in a sudden increase in particle size. Statistically, the influence of homogenisation time on particle size was found to be significant ($p<0.05$). Furthermore, the conversion rate increased as the homogenisation time increased. Meanwhile, the encapsulation rate increased initially and then decreased, with the maximum value (91.4 %) observed at 12 min.

The effect of the BSA/PTX ratio on albumin nanoparticles is shown in fig. 3f. When the BSA/PTX ratio decreased from 25 to 5 (dosage increases), the conversion rate and particle size increased; however, the encapsulation efficiency decreased. This indicates that the amount of BSA was not sufficient to encapsulate the entire loaded PTX amount. Similarly, when the dosage increased, the drug acted as a coagulant, resulting in many crystalline nuclei. At this time, BSA was adsorbed, resulting in particle adherence and large particles[24]. Statistically, the BSA/PTX ratio was found to significantly influence the encapsulation efficiency ($p<0.05$).

Finally, the following reaction conditions were deemed to be optimal-BSA concentration is 10 mg/ml, $MgCl_2$ is 0.5 mg/ml, water/ethanol volume ratio is 20/1, homogenisation pressure is 800 bar, homogenisation time is 3 min and BSA/PTX is 10/1.

The morphology of BSA-PTX nanoparticles were analyzed using TEM and SEM, as shown in fig. 4. It can be seen in the SEM images (fig. 4a) that albumin is in the form of irregular flakes while raw PTX is in the form of crystalline strips (fig. 4b). It can also be concluded from the SEM images (fig. 4c and fig. 4d) of BSA-PTX nanoparticles that the freeze-dried particles were mostly in the form of dimers and trimers with an average particle size of 300 nm; in terms of shape, most single particles were spherical. The TEM image of BSA-PTX nanoparticles (fig. 4e) shows that the freeze-dried powder consisted of nearly spherical nanoparticles with an average particle size of 300 nm. Fig. 4f shows larger size (about 500 nm) particles, there are obvious black crystals in the middle of the particles; these are assumed to be cores formed by $MgCl_2$ (coagulant). During the formation of albumin nanoparticles, the coagulant formed the core and albumin shells were formed around

them. Faint PTX crystal strips could also be observed, implying that PTX was dispersed in the carrier in the form of crystals.

FTIR can be used to easily detect the relative intensity of amide bands in proteins, thus allowing us to analyse their structure. We employed FTIR to analyse the structure of albumin nanoparticles and investigate changes in their characteristic absorption peaks to determine their composition (fig. 5). The Infrared Spectroscopy (IR) spectrum of albumin included characteristic peaks at 1638, 1540, and 1238 cm^{-1}, representing amide I (1600-1700 cm^{-1}, C=O stretching vibrations), amide II (1500-1600 cm^{-1}, N-H in-plane bending and C-N stretching), and amide III (1220-1280 cm^{-1}, C-N stretching and N-H in-plane bending) groups, respectively. The appearance of these peaks is mainly due to the fact that albumin is in a disordered coiled state[25]. It can be seen from the figure that the absorption band of amide I moved from 1638 to 1654 cm^{-1} after albumin was micronized, which may be due to the rearrangement of amino and carboxyl hydrogen bonds on the BSA peptide chain during the homogenisation process. Protein conformation undergoes changes once hydrogen bonds, which are the main forces responsible for the double helix structure in a protein change[26]. No obvious changes could be observed in the FTIR spectrum of BSA, but the peak intensity corresponding to amide II (1540 cm^{-1}) increased significantly, indicating that the C-N and/or N-H bonds underwent changes due to interactions between different functional groups[27]. An obvious characteristic peak could be observed in the FTIR spectrum of $MgCl_2$ at 2250 cm^{-1}; however, it could not be observed in the spectra of $MgCl_2$ blank nanoparticles and $MgCl_2$ drug-loaded nanoparticles. This implies that the $MgCl_2$ amount is so small that it has little effect on drug-loaded nanoparticles. The PTX spectrum included a ketocarbonyl (C=O) stretching vibration peak at 1733 cm^{-1}, which could also be observed in the spectrum of $MgCl_2$ drug-loaded nanoparticles. Thus, FTIR validated

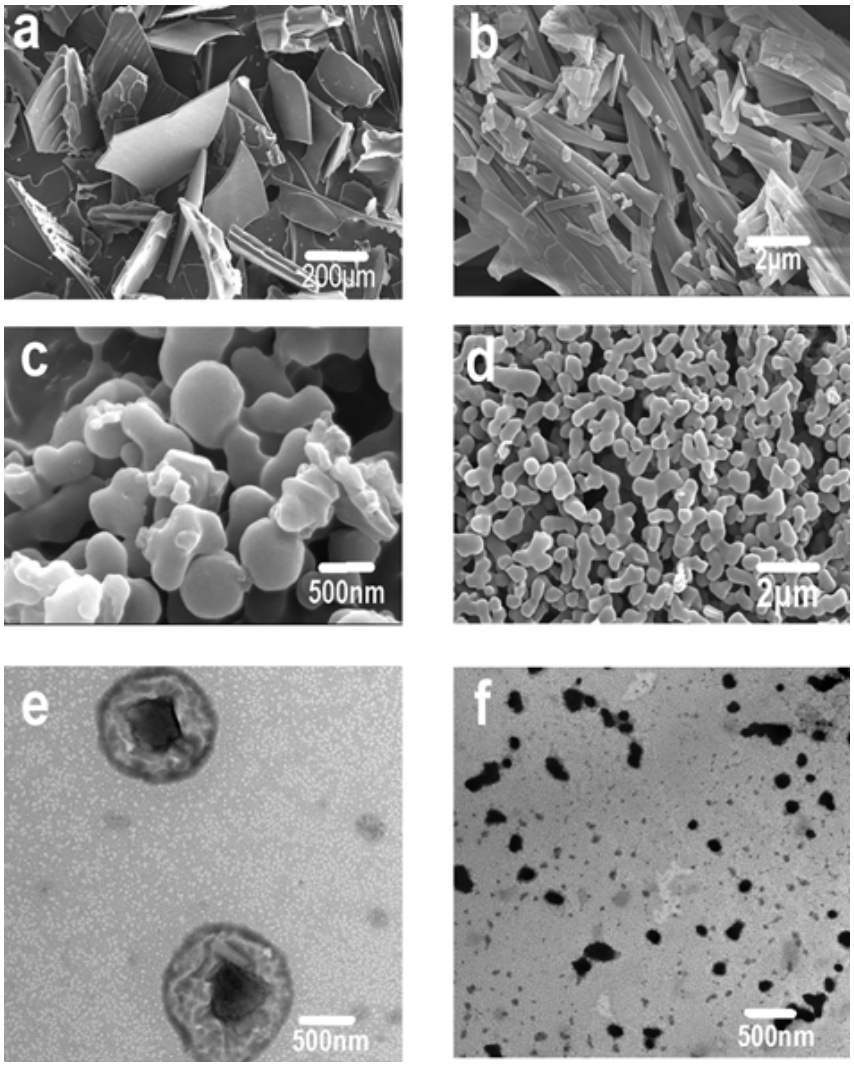

Fig. 4: (a) Scanning electron micrographs of BSA; (b) PTX; (c and d) BSA-PTX and (e and f) TEM of BSA-PTX

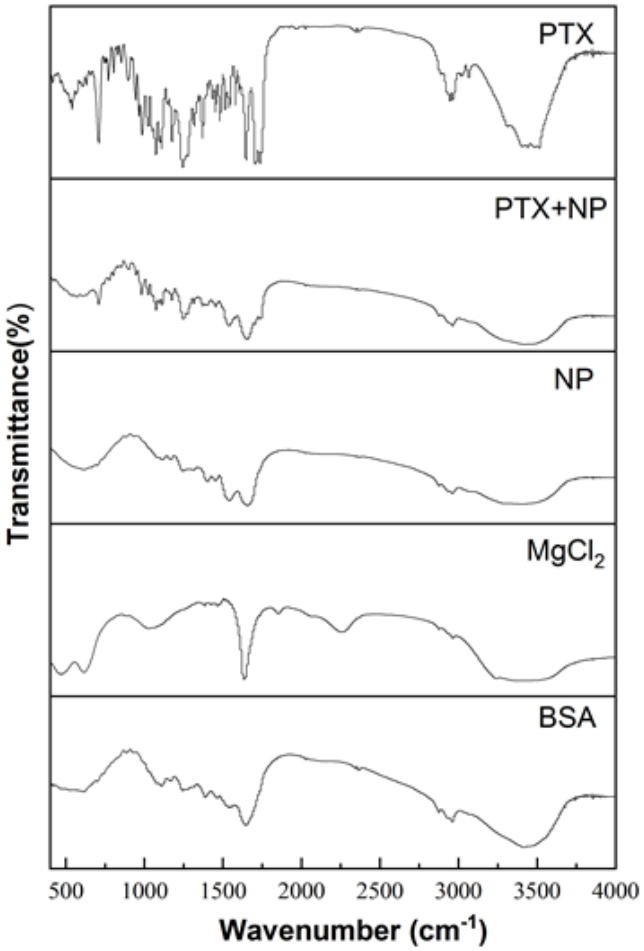

Fig. 5: FTIR spectra of BSA; $MgCl_2$; nanoparticle; PTX-BSA and PTX. The characteristic vibration bands related to BSA and PTX can be seen in the PTX-BSA NPs nanoparticles

PTX encapsulation in albumin.

Raman spectroscopy is a rapid, simple, repeatable and non-destructive qualitative and quantitative technique that does not require special sample preparation. Thus, we employed this method to analyse the BSA-based nanoparticles prepared in this study. As shown in fig. 6, peaks were observed at 1655 and 1339 cm^{-1} in the spectrum corresponding to albumin, representing amide I and III groups[28]. After nanoparticle formation, the relative intensities of these peaks decreased. This phenomenon can be explained by the structural changes occurring during the formation of BSA nanoparticles[29]. S-S stretching vibrations were observed in the wavenumber range of 500-550 cm^{-1} and these can be used to evaluate the configuration characteristics of disulphide bonds. The Raman peak at 510 cm^{-1} is characteristic of the double-twist configuration. Upon nanoparticle formation, Raman peaks were observed at 525 cm^{-1} corresponding to twist-twist-trans and trans-twist-twist configurations, indicating changes in the disulphide bond configuration and protein structure.

The DSC curves of BSA, $MgCl_2$, blank nanoparticles, $MgCl_2$ drug-loaded nanoparticles and PTX are shown in fig. 7. A wide endothermic peak could be observed in the thermo gram of albumin at ~222°; however, this peak shifted to 197° and widened in the thermo gram of $MgCl_2$ drug-loaded nanoparticles. Data analysis showed that albumin was denatured during nanoparticle formation, which is consistent with related reports[30]. PTX exhibited an endothermic peak at ~219°, which corresponds to its melting point, indicating that the drug exists in a crystalline state. However, no characteristic endothermic peaks could be observed at this temperature in the thermo gram of BSA-PTX nanoparticles, indicating that the drug underwent phase transformation and converted into an amorphous structure (low drug contents might also be responsible for this observation). It is well known that polymers retard crystalline growth in drugs *via* surface adsorption. Thus, the disappearance of the PTX melting

peak indicates that PTX crystallisation was inhibited by albumin during precipitation[31].

XRD was conducted to investigate structural changes in the drug and albumin during nanoparticle preparation (fig. 8). Pure PTX exhibited a strong diffraction peak, indicating its crystalline nature. In contrast, BSA was present in an amorphous state, as described in other studies[32]. Multiple diffraction peaks can be seen in the XRD patterns of blank and drug-loaded nanoparticles, which is not the case in the XRD patterns of albumin nanoparticles obtained by different methods. This difference might be due to the binding of $MgCl_2$ and albumin[33,34]. Furthermore, the original diffraction peaks of PTX could not be observed in the XRD patterns of the nanoparticles, suggesting that drug converted into an amorphous state[1].

The effect of different crosslinking agents (genipin, vanillin and glutaraldehyde) on drug release from the nanoparticles in *in vitro* conditions was investigated[35]. BSA-PTX nanoparticles were immersed in PBS (pH 7.4) at 37° for 24 h *in vitro* and the amount of drug released was analyzed (fig. 9). While genipin (20 mg) and vanillin (13.45 mg) and glutaraldehyde (1.6 ml, 0.1 %) was added at a concentration of 4 µl/mg albumin and the crosslinking time was set at 3 h. A sustained release could be observed with cross linked BSA-PTX nanoparticles, whereas non-cross linked BSA-PTX nanoparticles exhibited a rapid release, with a 37 % initial release within 15 min. The release rate reached 97 % within 4 h after which it converted into a plateau. When the nanoparticles were in contact with the release medium, the drug adsorbed on nanoparticle surfaces was first dissolved and released, resulting in a burst-release effect. At 1 h, the cumulative release rate was in the range of 42.61 % to 59.32 %. Subsequently, the release rate increased to 82.92 % to 91.70 % within 6 h, after which it gradually slowed down (plateau phase). The release mode was biphasic, i.e. a burst effect at the beginning followed by a slow release phase. The release medium continuously penetrated the interior of the nanoparticles, resulting in the release of drug molecules embedded in their bulk. The dissolved drug diffused into the medium through carriers depending on the drug-concentration gradient inside and outside the particles; when accompanied by the slow dissolution of the carrier material, this resulted in a slow release. Such sustained release behavior can be attributed to the decrease in the free volume of the matrix treated with the crosslinking agents and $MgCl_2$,

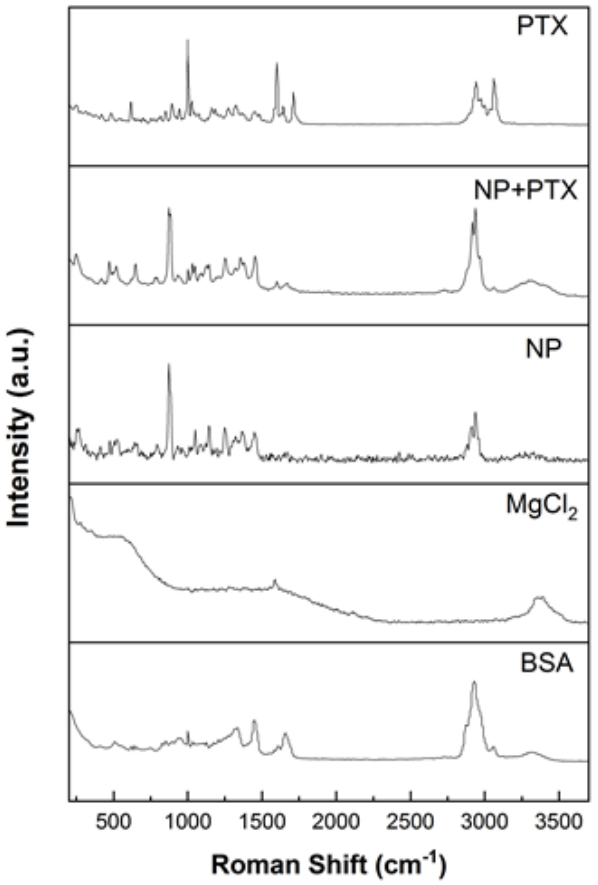

Fig. 6: Raman spectrum of BSA; $MgCl_2$; nanoparticle; PTX-BSA and PTX

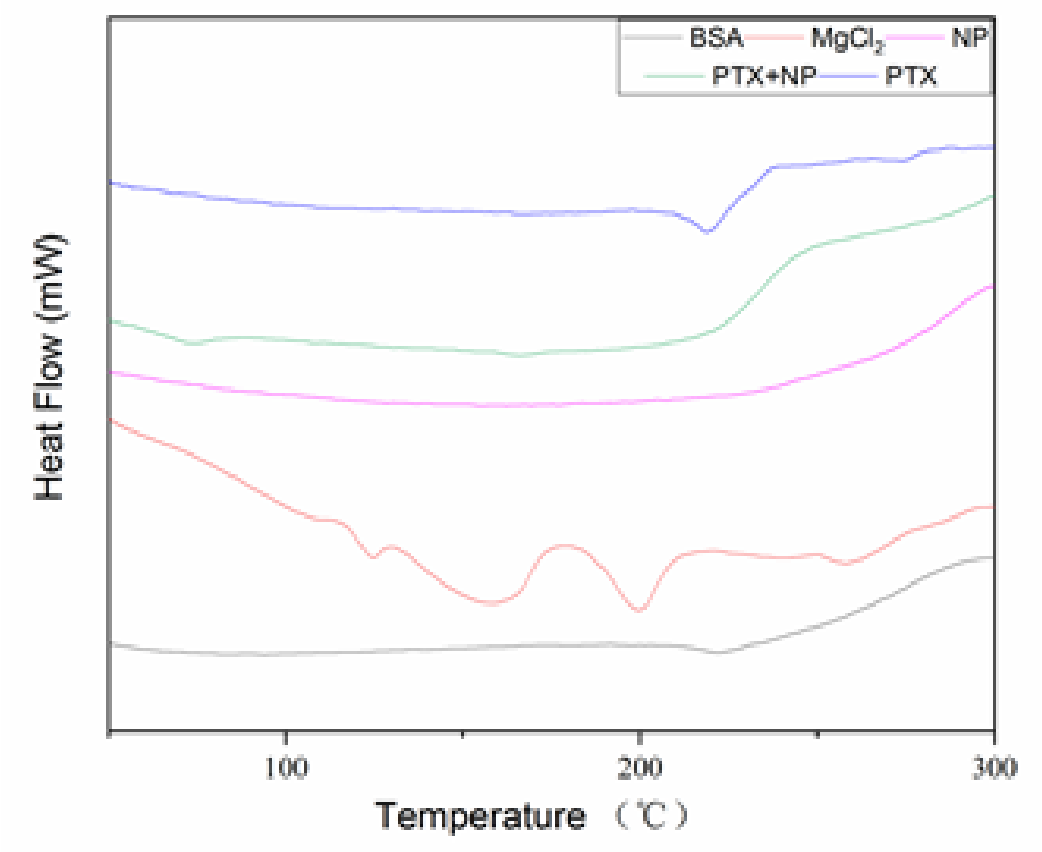

Fig. 7: The DSC thermogram of BSA; $MgCl_2$; nanoparticle; PTX-BSA and PTX

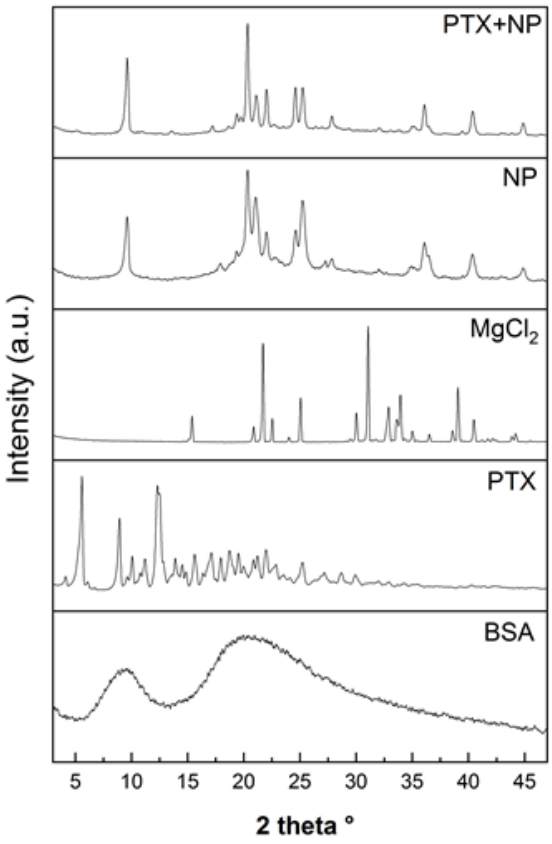

Fig. 8: The XRD spectra of BSA; $MgCl_2$; nanoparticle; PTX-BSA and PTX

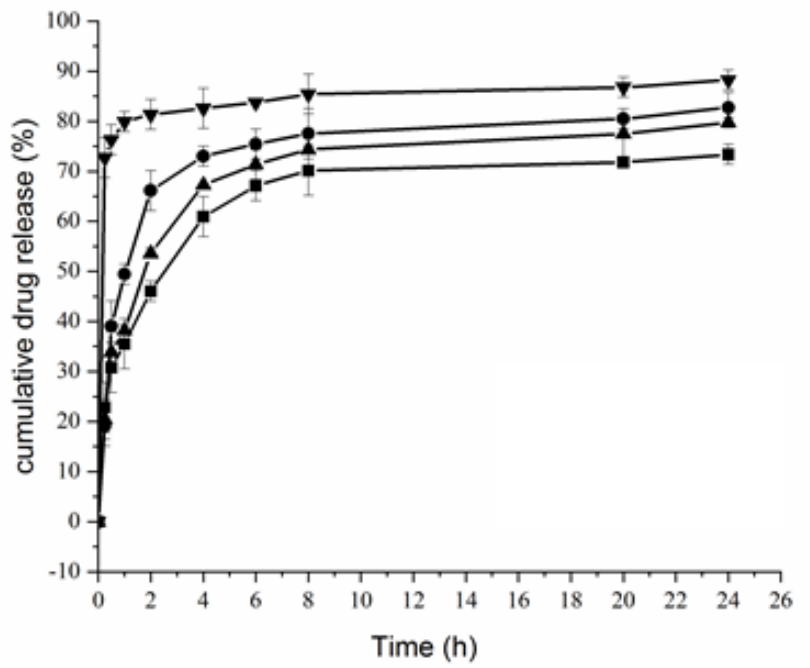

Fig. 9: *In vitro* release profiles of PTX from PTX-BSA. Crosslinking agent dosage, glutaraldehyde/BSA 0.4 µl/mg; genipin/BSA 0.05 mg/mg and vanillin/BSA 0.02 mg/mg
Note: (–■–): Vanillin; (–●–): Genipin; (–▲–): Glutaraldehyde and (–▼–) : No cross linker

which may limit the diffusion of drugs into the protein network. The observed release rate followed the trend, genipin group>glutaraldehyde group>vanillin group.

In this study, a new green method called HPHCM was developed for the preparation of albumin nanoparticles. The effect of different coagulants on the particle size and conversion rate of albumin nanoparticles was evaluated and it was found that $MgCl_2$ resulted in small particles and a high albumin-conversion rate. It was proved by single-factor experiments that BSA concentration; coagulant concentration, and homogenisation time influence the size of albumin nanoparticles, albumin-conversion rate and encapsulation rate. SEM analysis indicated that the prepared albumin nanoparticles were spherical with an average size of 300 nm and easily formed dimers or trimers upon lyophilisation. DSC testing showed that albumin mainly existed in an amorphous form after nanoparticle formation. The peak shift corresponding to amide I in the FTIR spectrum of the nanoparticles is evidence of changes in protein conformation. Using Raman spectroscopy, these changes were ascribed to changes in the disulphide bond configuration and protein structure. *In vitro* release studies confirmed sustained release from cross linked BSA-PTX nanoparticles for over 6 h. In terms of the cross linking agent, the release rate followed the order genipin>glutaraldehyde>vanillin. Finally, HPHCM is a simple and feasible method with great potential to synthesise drug carriers. It should be noted that BSA was used in this study with only four coagulants and three cross-linking agents. Therefore, other kinds of albumin, coagulants and cross-linking agents should also be studied to develop efficient drug carriers for targeted delivery.

Acknowledgements:

The authors gratefully acknowledge the financial supports of the National Natural Science Foundation of China (Grant No. 21908119) and the Natural Science Foundation of Heilongjiang Province of China (Grant No. H2016097).

Conflict of interests:

The authors declared no conflict of interest.

REFERENCES

1. Ruttala HB, Ko YT. Liposome encapsulated albumin-paclitaxel nanoparticle for enhanced antitumor efficacy. Pharm Res 2015;32(3):1002-16.
2. Dang Y, Guan J. Nanoparticle-based drug delivery systems for cancer therapy. Smart Mater Med 2020;1:10-9.
3. Thao LQ, Byeon HJ, Lee C, Lee S, Lee ES, Choi YW, *et al.* Doxorubicin-bound albumin nanoparticles containing a TRAIL protein for targeted treatment of colon cancer. Pharm Res 2016;33(3):615-26.
4. Karami E, Behdani M, Kazemi-Lomedasht F. Albumin nanoparticles as nanocarriers for drug delivery: Focusing on antibody and nanobody delivery and albumin-based drugs. J Drug Deliv Sci Technol 2020;55:101471.
5. Nosrati H, Salehiabar M, Manjili HK, Danafar H, Davaran S.

Preparation of magnetic albumin nanoparticles *via* a simple and one-pot desolvation and co-precipitation method for medical and pharmaceutical applications. Int J Biol Macromol 2018;108:909-15.
6. Kratz F. Albumin as a drug carrier: Design of prodrugs, drug conjugates and nanoparticles. J Control Release 2008;132(3):171-83.
7. Zu Y, Meng L, Zhao X, Ge Y, Yu X, Zhang Y, *et al.* Preparation of 10-hydroxycamptothecin-loaded glycyrrhizic acid-conjugated bovine serum albumin nanoparticles for hepatocellular carcinoma-targeted drug delivery. Int J Nanomed 2013;8:1207-22.
8. Steinhauser IM, Langer K, Strebhardt KM, Spänkuch B. Effect of trastuzumab-modified antisense oligonucleotide-loaded human serum albumin nanoparticles prepared by heat denaturation. Biomaterials 2008;29(29):4022-8.
9. Kim B, Lee C, Lee ES, Shin BS, Youn YS. Paclitaxel and curcumin co-bound albumin nanoparticles having antitumor potential to pancreatic cancer. Asian J Pharm Sci 2016;11(6):708-14.
10. Kouchakzadeh H, Safavi MS, Shojaosadati SA. Efficient delivery of therapeutic agents by using targeted albumin nanoparticles. Adv Protein Chem Struct Biol 2015;98:121-43.
11. Langer K, Balthasar S, Vogel V, Dinauer N, von Briesen H, Schubert D. Optimization of the preparation process for human serum albumin (HSA) nanoparticles. Int J Pharm 2003;257(1-2):169-80.
12. Koenig SG, Dillon B. Driving toward greener chemistry in the pharmaceutical industry. Curr Opin Green Sustain Chem 2017;7:56-9.
13. Sharma RK, Gulati S, Mehta S. Preparation of gold nanoparticles using tea: A green chemistry experiment. J Chem Edu 2012;89(10):1316-8.
14. Karthika S, Radhakrishnan TK, Kalaichelvi P. Crystallization and kinetic studies of an active pharmaceutical compound using ethyl lactate as a green solvent. ACS Sustain Chem Eng 2019;8(3):1527-37.
15. Sevilla P, Hernández M, Corda E, García-Ramos JV, Domingo C. Characterization molecular de nanoportadores de fármacos mediate espectroscopía intensificada poor Plasmon's localizes: Fluorescence (SEF) y Raman (SERS). Pure Appl Opt 2013;46:111-9.
16. Wang W, Lei Y, Sui H, Zhang W, Zhu R, Feng J, *et al.* Fabrication and evaluation of nanoparticle-assembled BSA microparticles for enhanced liver delivery of glycyrrhetinic acid. Artif Cells Nanomed Biotechnol 2017;45(4):740-7.
17. Galisteo-González F, Molina-Bolívar JA. Systematic study on the preparation of BSA nanoparticles. Colloids Surf B Biointerfaces 2014;123:286-92.
18. Prajapati A, Srivastava A. Preparation, characterization and encapsulation efficiency of egg albumin nanoparticles using EDC as cross linker. J Sci Ind Res 2019;78:703-5.
19. Shu S, Zhang X, Teng D, Wang Z, Li C. Polyelectrolyte nanoparticles based on water-soluble chitosan–poly (l-aspartic acid)–polyethylene glycol for controlled protein release. Carbohydr Res 2009;344(10):1197-204.
20. Dang F, Enomoto N, Hojo J, Enpuku K. Sonochemical synthesis of monodispersed magnetite nanoparticles by using an ethanol–water mixed solvent. Ultrason Sonochem 2009;16(5):649-54.
21. Fayaz AM, Balaji K, Kalaichelvan PT, Venkatesan R. Fungal based synthesis of silver nanoparticles-An effect of temperature on the size of particles. Colloids Surf B Biointerfaces 2009;74(1):123-6.
22. Jenning V, Lippacher A, Gohla SH. Medium scale production of solid lipid nanoparticles (SLN) by high pressure homogenization. J Microencapsul 2002;19(1):1-10.
23. Yazdani F, Edrissi M. Effect of pressure on the size of magnetite nanoparticles in the coprecipitation synthesis. Mater Sci Eng B. 2010;171(1-3):86-9.
24. Yang L, Cui F, Cun D, Tao A, Shi K, Lin W. Preparation, characterization and biodistribution of the lactone form of 10-hydroxycamptothecin (HCPT)-loaded bovine serum albumin (BSA) nanoparticles. Int J Pharm 2007;340(1-2):163-72.
25. Tang J, Luan F, Chen X. Binding analysis of glycyrrhetinic acid to human serum albumin: Fluorescence spectroscopy, FTIR and molecular modeling. Bioorg Med Chem 2006;14(9):3210-7.
26. Shi X, Li D, Xie J, Wang S, Wu Z, Chen H. Spectroscopic investigation of the interactions between gold nanoparticles and bovine serum albumin. Chin Sci Bull 2012;57(10):1109-15.
27. Bronze-Uhle ES, Costa BC, Ximenes VF, Lisboa-Filho PN. Synthetic nanoparticles of bovine serum albumin with entrapped salicylic acid. Nanotechnol Sci Appl 2017;10:11-21.
28. Bhogale A, Patel N, Mariam J, Dongre PM, Miotello A, Kothari DC. Comprehensive studies on the interaction of copper nanoparticles with bovine serum albumin using various spectroscopies. Colloids Surf B Biointerfaces 2014;113:276-84.
29. Rohiwal SS, Satvekar RK, Tiwari AP, Raut AV, Kumbhar SG, Pawar SH. Investigating the influence of effective parameters on molecular characteristics of bovine serum albumin nanoparticles. Appl Surface Sci 2015;334:157-64.
30. Taheri A, Atyabi F, Salman Nouri F, Ahadi F, Derakhshan MA, Amini M, *et al.* Nanoparticles of conjugated methotrexate-human serum albumin: Preparation and cytotoxicity evaluations. J Nanomater 2011;2011.
31. Honary S, Jahanshahi M, Golbayani P, Ebrahimi P, Ghajar K. Doxorubicin-loaded albumin nanoparticles: Formulation and characterization. J Nanosci Nanotechnol 2010;10(11):7752-7.
32. Ruttala HB, Ramasamy T, Shin BS, Choi HG, Yong CS, Kim JO. Layer-by-layer assembly of hierarchical nanoarchitectures to enhance the systemic performance of nanoparticle albumin-bound paclitaxel. Int J Pharm 2017;519(1-2):11-21.
33. Wang D, Liang N, Kawashima Y, Cui F, Yan P, Sun S. Biotin-modified bovine serum albumin nanoparticles as a potential drug delivery system for paclitaxel. J Mater Sci 2019;54(11):8613-26.
34. Zhao Y, Cai C, Liu M, Zhao Y, Wu Y, Fan Z, *et al.* Drug-binding albumins forming stabilized nanoparticles for co-delivery of paclitaxel and resveratrol: *In vitro*/*in vivo* evaluation and binding properties investigation. Int J Biol Macromol 2020;153:873-82.
35. Elzoghby AO, Samy WM, Elgindy NA. Albumin-based nanoparticles as potential controlled release drug delivery systems. J Control Release 2012;157(2):168-82.